Original Article

DOI: 10.5582/ddt.2025.01023

Generation and characterization of a humanized GJB2 p.V37I knock-in mouse model for studying age-related hearing loss

Yiding Yu[1,2,3], Yue Li[1,2,3], Jingyun Li[1,2,3], Xu Zhang[1,2,3], Xuemin Chen[4,5], Pengzhao Hu[4,5], Wenjie Huang[4,5], Cheng Wen[1,2,3], Lin Deng[1,2,3], Xiaohua Cheng[1,2,3], Ning Yu[4,5,*], Lihui Huang[1,2,3,*]

[1] Otolaryngology Head and Neck Surgery, Beijing Tongren Hospital, Capital Medical University, Beijing, China;
[2] Beijing Institute of Otolaryngology, Beijing, China;
[3] Key Laboratory of Otolaryngology Head and Neck Surgery, Ministry of Education, Beijing, China;
[4] College of Otolaryngology Head and Neck Surgery, Chinese PLA General Hospital, Beijing, China;
[5] National Clinical Research Center for Otolaryngologic Diseases, Beijing, China.

SUMMARY: Age-related hearing loss (ARHL) has been closely linked to genetic factors, with studies identifying the p.V37I mutation in the *GJB2* gene as a potential contributor to ARHL. To investigate this, we generated a humanized p.V37I mutant mouse model and performed auditory brainstem response (ABR) testing, cochlear morphology assessments, and transcriptional sequence of mutant and wild-type (WT) mice at different ages. Our results indicated that this kind of *GJB2* mutation does not lead to cochlear developmental abnormalities, and aging mutant mice exhibit only mild hearing loss compared to WT mice, without significant cochlear morphological differences. However, transcriptional analyses revealed substantial differences between mutant and WT mice. GO enrichment analysis of the DEGs between aging mutant and WT mice highlights significant enrichment in biological processes related to neural and sensory functions. Notably enriched terms include "neuron-to-neuron synapse," "immune response-activating signaling pathway," "regulation of synapse structure or activity," and "sensory perception of sound." These findings suggest that the p.V37I mutation in aging mice affects synaptic and calcium signaling pathways, as well as sensory system development. Despite these molecular changes, cochlear function remains normal in early life; however, as the mice age, hearing loss accelerates, likely due to a diminished capacity for gene-mediated protection against external stimuli.

Keywords: Age-related hearing loss, genetic hearing loss, c.109G>A mutant, RNA-seq, knock-in mouse

1. Introduction

Age-related hearing loss (ARHL) is a significant public health concern, affecting over 1.5 billion people worldwide, with about one-third of those over 65 experiencing disabling hearing loss (*1*). Beyond the auditory deficits, ARHL is associated with cognitive decline, increased risks of falls, depression, loneliness, and dementia (*2-4*), collectively imposing significant social and economic burdens. These challenges underscore the urgent need for effective prevention and treatment strategies (*5,6*).

ARHL is thought to result from the interplay of multiple factors, including aging, environmental influences, and genetics, with genetic factors accounting for 30% to 70% of cases (*1,7*). Among the genetic contributors, *GJB2* is the most well-known deafness-associated gene, responsible for over 50% of sensorineural hearing loss (SNHL) cases and a primary target in newborn genetic screening (*7*). While *GJB2*'s role in congenital hearing loss is well-recognized, its contribution to hearing loss in adults, particularly in the elderly, is increasingly being appreciated. One specific mutation, p.V37I (c.109G>A), has been shown to be ethnically specific, with a high carrier rate (6.2-11.79%) in the Chinese population (*8,9*). Importantly, this mutation has been implicated in age-related hearing loss (*10*).

Although nearly all newborns in China undergo genetic and hearing screening at birth these years (*11,12*), adults are rarely tested for the genetic causes of hearing loss, even though approximately 80% of hearing loss cases are diagnosed after the second decade of life (*1*). This gap in genetic testing among adults highlights the need to better understand the genetic underpinnings of ARHL to guide future diagnostic and therapeutic strategies. Given the high carrier rate of the p.V37I (c.109G>A) mutation, its investigation holds significant

clinical relevance.

Due to the limited availability of human cochlear samples, it is essential to develop appropriate animal models to effectively investigate the pathogenesis of hearing loss caused by gene mutations. Currently, there have been studies on animal models of the *GJB2* gene c.109G>A mutation, particularly the p.V37M mouse model (*13,14*). However, a p.V37I model with the same mutation as in humans has not been established. In this study, we have successfully created a p.V37I mouse model for the first time by performing precise double-base editing at the p.V37 codon of the *GJB2* gene. This model is expected to provide a foundation for the future development of therapeutic and preventive strategies for hearing loss.

2. Materials and Methods

2.1. Generation of the p.V37I knock-in mouse model

Mice were generated from the C57BL/6J background. The p.V37I knock-in mice were generated using the CRISPR/Cas9 genome editing system. The efficacy of the target site was verified using the spCas9-gRNA Target Efficiency Assay Kit (Beijing, China). The guide RNA (gRNA) and Cas9 were expressed in the vector (Figure 1A). The mouse *GJB2* gene sequences were obtained from NCBI (National Center of Biotechnology Information,Gene ID:14619). Given that the c.109G>A mutation differ between humans and mice, a direct c.109G>A substitution in mice would result in a p.V37M amino acid change, to achieve the desired p.V37I amino acid substitution, we modified two distinct DNA bases (Figure 1B). The Cas9 Nickase mRNA, Cas9 target gRNA, and donor DNA were microinjected into mouse zygotes under standard conditions to generate the F0 generation. F1 offspring carrying the heterozygous p.V37I mutation were obtained by crossing mutant founders (F0) with C57BL/6J. After the birth of founder

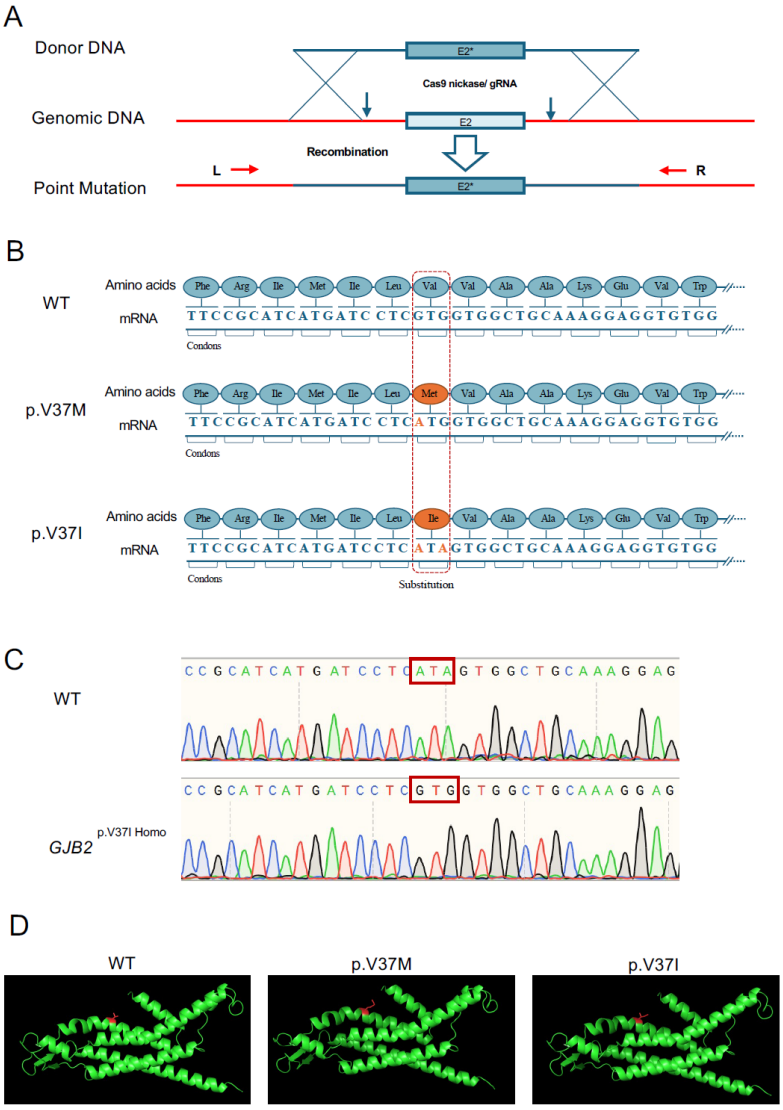

Figure 1. The generation of p.V37I mice. A: Schematic diagram of the construction of the p.V37I mutation mice. **B**: The difference of the amino acids and mRNA sequence between WT, p.V37M and p.V37I variants. **C**: Representative Sanger sequencing results confirming the p.V37I mutation in mice. **D**: Three-dimensional structural modeling and visualization of *GJB2* protein variants.

mice, tail samples were collected for DNA extraction, followed by PCR and sequencing to identify positive founders. F2 offspring with the homozygous p.V37I mutation were generated from the crossing between heterozygous F1 offspring. The genotyping of the homozygous mice we produced was confirmed using PCR analysis and Sanger sequencing of genomic DNA extracted from mouse tail clippings to detect the targeted mutation (Figure 1C). All animal procedures adhered to guidelines for animal research and were approved by the Experimental Animal Ethics Committee of Capital Medical University (Number: TRLAWEC2022-S186).

2.2. Functional predictions of *GJB2* mutations

The functional effects of the p.V37I and p.V37M mutations on the GJB2 protein were evaluated using two widely used mutation prediction tools, SIFT (*https://sift.bii.a-star.edu.sg/*) and PolyPhen-2 (*http://genetics.bwh.harvard.edu/pph2/*), with default threshold settings. The GJB2 protein sequence (UniProtKB-Q00977) was used as the query. To further investigate the structural impacts of the p.V37I and p.V37M mutations, we employed PyMOL for three-dimensional structural modeling and visualization of both mutant (p.V37I&p.V37M) and wild-type proteins. The secondary structure was rendered, with α-helices displayed in green. The mutation sites – methionine at position 37 for p.V37M and isoleucine for p.V37I – were highlighted in red to illustrate their locations within the protein and spatial relationships with surrounding residues. High-resolution rendering was performed to generate structural images for analysis and presentation.

2.3. Auditory brainstem response tests

Auditory brainstem response (ABR) tests were performed in WT ($n = 6$) and homozygous p.V37I ($n = 6$) mice every month between the ages of 1 month and the 12 months. The mice were anesthetized with 1% sodium pentobarbital (50 mg/kgb.w.) delivered intraperitoneally. The anesthetized mice were moved into the shielded room, the electrodes were connected. We use the TDT system to measure the thresholds of the auditory brainstem response (ABR) in mice. The active electrodes were inserted into the vertex and the ipsilateral retro-auricular region with a ground electrode on the back of the mouse's head. Specifically, the ABR threshold for pure-tone stimuli was measured at frequencies of 8, 16, and 24 kHz. Experimental animals were tested for ABR thresholds at each frequency of Click, 8 kHz, 16 kHz, and 24 kHz, with stimulus intensities starting at 90 dB SPL and decreasing in 10 dB increments, and thresholds were judged by the lowest stimulus intensity at which repeatable wave II could be discerned. The genotypes of the mice were kept confidential from the tester during the experiment.

2.4. Cochlear histology analysis

Fresh cochleae were perfused with 4% paraformaldehyde (Solarbio, Beijing, China) in PBS through small openings at the apex and base, repeated more than three times until lymphatic fluid mixed with blood was expelled. The cochleae were then transferred into an Eppendorf tube containing the paraformaldehyde overnight at 4°C. The 10% EDTA solution (Solarbio, Beijing, China) was used for decalcification at room temperature for 24 hours. For light microscopy studies, the samples were dehydrated and embedded in paraffin. Subsequently, serial sections (5 mm) were stained with H&E.

2.5. Immunofluorescence

After decalcification with disodium EDTA, the cochleae were dehydrated with 15% and 30% sucrose for 1.5 h each and embedded in optimal cutting temperature compound (Sakura, CA, USA) overnight at 4°C. And sections with a thickness of 10 μm were cut. Meanwhile, the sensory epitheliums of cochlea were dissected out and were incubated in blocking solution (containing 10% goat serum, 1% BSA), and 0.1% Triton X-100 in PBS for 30 minutes. The epitheliums were incubated overnight at 4°C with monoclonal mouse anti-Cx26 antibody (1:400, Invitrogen, CA, USA) prepared in the blocking solution. For double immunofluorescence staining of Cx26 and Cx30, polyclonal rabbit anti-Cx30 antibody (1:400, CA, USA) was used. After being washed with PBS three times, the epithelium sections were incubated with corresponding Alexa Fluor 488- and 568-conjugated goat anti-mouse IgG and Alexa Fluor 568-conjugated goat anti-rabbit IgG (1:500, Thermofisher, MA, USA) in the blocking solution at room temperature (25°C) for 1 hour. The sections were stained by 4′, 6-diamidino-2-phenylindole (DAPI, 0.1 mg/mL, D1306; Thermofisher, MA, USA) for 15 minutes to visualize cell nuclei. A confocal microscope (Zeiss, Germany) was used to observe the experimental results.

2.6. Scanning electron microscope

After decalcification with 10% EDTA decalcification solution, the cochlear epitheliums were exposed by dissection, and the fixed sample was rinsed three times for 15 min each in 0.1 M phosphate buffer PB (pH 7.4). 1% osmium acid prepared in 0.1 M phosphate buffer PB was fixed at room temperature and protected from light for 1.5 h. The sample was then rinsed three times for 15 min each in 0.1 M phosphate buffer PB. The cochlear tissues were then dehydrated in gradient alcohol and dried for 15 min after the transition to isoamyl acetate, and the samples were placed in a critical point dryer (Quorum, UK) and coated by ion sputtering vacuum coating. An electron microscope (Hitachi, Japan) was used for observation and photography.

2.7. RNAseq

Samples were subjected to total RNA using Trizol (Invitrogen, CA, USA) according to the protocol outlined by Chomczynski *et al.* (*15*). RNA quality was determined by A260/A280 measuring using a NanodropTM One C spectrophotometer (ThermoFisher, MA, USA). Quantification of qualifying RNAs was performed using a Qubit3.0 with a QubitTM RNA Broad Range Assay kit (Life Technologies, CA, USA). The stranded RNA sequencing library was prepared using a KC-DigitalTM Stranded mRNA Library Prep Kit for Illumina® (Seqhealth Technology Co., Ltd. Wuhan, China) following the manufacturer's instructions. Finally sequenced on an Illumina Novaseq 6000 platform.

2.8. Statistical analysis

All tests, tissue processing, quantification, and data analysis were conducted in a blinded manner throughout the study. To assess the normality of the data distribution, parametric tests (unpaired two-tailed Student's *t*-test) were used (GraphPad Prism 8.0). The data are expressed as the mean ± SEM and statistical significance was defined as $P < 0.05$.

2.9. Bioinformatic analysis

2.9.1. Screening of differentially expressed genes

The gene expression in the p.V37I mice and the wild-type (WT) mice, the sequence reads were then mapped to the mouse genome assembly (GRCm38/mm10) using STAR v2.5.3a. Following this, the differential gene expression between p.V37I and wild-type mice analysis was performed using the DESeq2 (*16*), with a screening condition of *P*-adjusted < 0.05 and the |log2FC| > 1.5.

2.9.2. Functional annotation of the DEGs

The DEGs were analyzed for enrichment using Gene Ontology (GO) through clusterProfiler (4.6.2). The corresponding biological functions related to the differentially expressed genes (DEGs) were also presented. The calculated *P*-value was adjusted through Benjamini and Hochberg's approach, using an adjusted $P < 0.05$ as a threshold. GO terms with adjusted $P < 0.05$ were regarded as significantly enriched by DEGs.

3. Results

3.1. *GJB2* p.V37I and p.V37M mutations can cause potential functional impairment

SIFT analysis predicted both two variants to be "tolerated," with output scores of 0.22 for p.V37M and 0.67 for p.V37I, indicating a relatively lower likelihood of functional disruption. In contrast, PolyPhen-2 classified both mutations as "probably damaging," with a score of 1.000 for p.V37M (sensitivity: 0.00; specificity: 1.00) and 0.999 for p.V37I (sensitivity: 0.14; specificity: 0.99), suggesting a high probability of protein function alteration. Additionally, three-dimensional structural modeling and visualization revealed notable differences between the p.V37I and wild-type proteins, indicating that the p.V37M and p.V37I mutations may affect protein stability (Figure 1D).

3.2. The aged p.V37I knock-in mice have progressive mild hearing loss

The ABR assay was performed on p.V37I mice and wild-type mice, including Click, 8 kHz,16 kHz, and 32 kHz. We observed that the response thresholds of the p.V37I mice were mildly elevated when compared to those of the wild-type mice, particularly from 8 to 12 months of age. This elevation was most pronounced at higher frequencies ($P < 0.05$), as depicted in Figure 2A.

3.3. The p.V37I knock-in mice have normal cochlear development.

In adult p.V37I mice at 1 month of age, morphological assessments showed normal cochlear development, it indicated that this kind of mutation can't induce developmental disorder. The cochlear tunnel remained open, with no visible abnormalities or loss detected in the hair cells or the structural integrity of the organ of Corti (Figure 2B). Additionally, SEM analysis revealed no significant disruptions in cilium structure or arrangement (Figure 2C). These findings suggest that the p.V37I mutation does not significantly affect the morphological development of the cochlea and does not result in pronounced hair cell abnormalities.

3.4. The expression levels of Cx26 and Cx30 showed no significant changes

Cx26 and Cx30 are the predominant gap junction proteins in the cochlea. Immunofluorescence staining of 1-month-old (when the auditory system is developed) p.V37I mice revealed the presence of foveal gap junction structures on the supporting cell membrane, in which Cx26 and Cx30 were co-localized correctly (Figure 2D, 2E). The p.V37I mice did not exhibit any significant differences in the localization or overall expression pattern of these proteins compared to the wild-type group. This suggests that the single amino acid substitution at position 37 does not result in a major alteration in the expression or distribution of the proteins. Specifically, the p.V37I mutation did not appear to affect the normal expression or localization of Cx26, nor does it lead to protein retention in the cytoplasm.

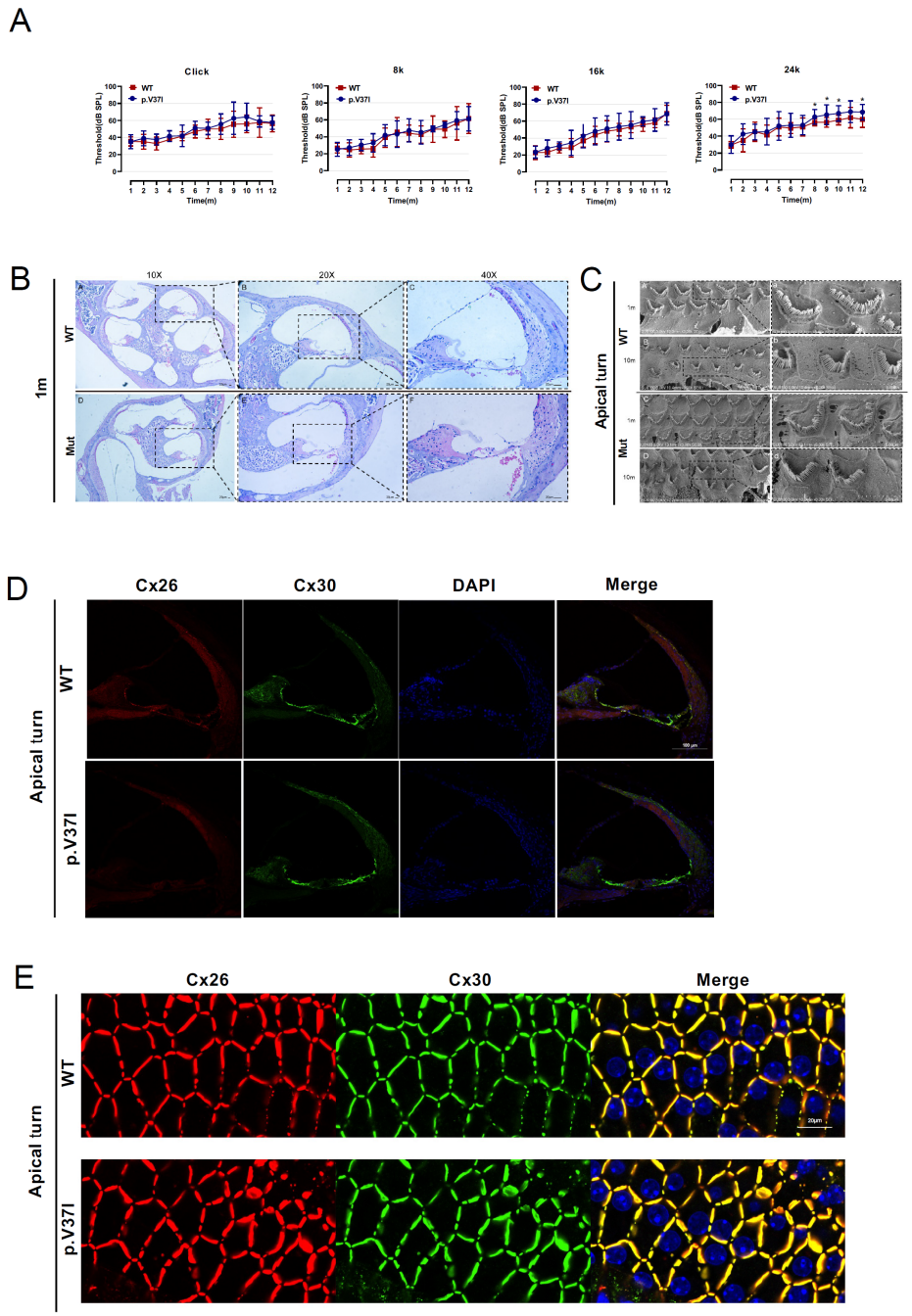

Figure 2. ABR thresholds and cochlea morphology of the p.V37I and wild-type (WT) mice. A: The averaged ABR thresholds of the wild-type and p.V37I mice at Click, 8, 16, and 24 kHz. The number of tested mice of each group is 6, asterisks indicate the statistical significance with P-values of 0.05 or lower. **B**: H&E staining showing the normal gross morphology of the p.V37I mice cochleae. Scale bars: 20 μm. **C**: Scanning electron microscopy showing normal cellular structure and arrangement of the hair cell in the p.V37I mice. **D**: Immunofluorescent staining for Cx26 (red) and Cx30 (green) in the cochlea. Scale bars: 100 μm. **E**: Immunofluorescent staining of Cx26 (red), Cx30 (green) and merged images at the age of 4 weeks from apical turns membrane. Scale bars: 20 μm.

3.5. Transcriptome analysis of the cochlea between the p.V37I mice and the WT mice.

We conducted a comparative analysis of gene expression in p.V37I and WT mice at both young (1-month) and old (8-month) ages. At 1 month, p.V37I mice exhibited 7 up-regulated and 1,311 down-regulated genes compared to wild-type mice, with an adjusted *P*-value < 0.05 and fold changes > 1.5. At 8 months, there were 1,269 up-regulated and 732 down-regulated genes in p.V37I mice relative to WT mice. Principal Component Analysis (PCA) revealed distinct clustering; at young ages, the expression profiles of p.V37I and WT mice overlapped, whereas at older ages, the profiles were clearly separable (Figure 3A). Differential expression was visualized using volcano plots (Figure 3B). GO enrichment analysis of the DEGs between aging p.V37I and WT mice highlighted significant enrichment in biological processes related to

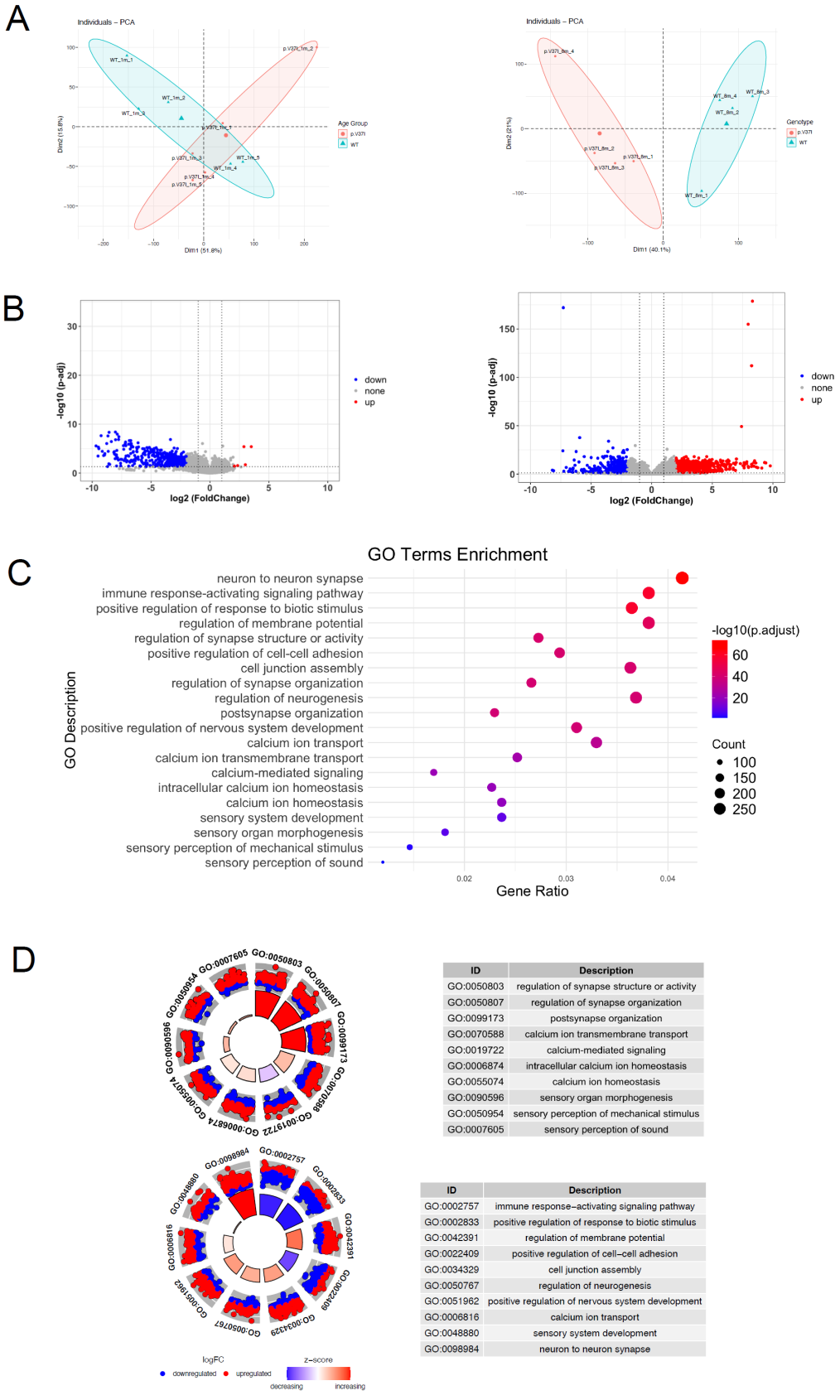

ID	Description
GO:0050803	regulation of synapse structure or activity
GO:0050807	regulation of synapse organization
GO:0099173	postsynapse organization
GO:0070588	calcium ion transmembrane transport
GO:0019722	calcium-mediated signaling
GO:0006874	intracellular calcium ion homeostasis
GO:0055074	calcium ion homeostasis
GO:0090596	sensory organ morphogenesis
GO:0050954	sensory perception of mechanical stimulus
GO:0007605	sensory perception of sound

ID	Description
GO:0002757	immune response–activating signaling pathway
GO:0002833	positive regulation of response to biotic stimulus
GO:0042391	regulation of membrane potential
GO:0022409	positive regulation of cell–cell adhesion
GO:0034329	cell junction assembly
GO:0050767	regulation of neurogenesis
GO:0051962	positive regulation of nervous system development
GO:0006816	calcium ion transport
GO:0048880	sensory system development
GO:0098984	neuron to neuron synapse

Figure 3. Transcriptome analysis of the cochlea between the p.V37I mice and the WT mice in different age. A: Principal Component Analysis (PCA) revealed the clustering of different cochlea group, at older age, the transcript profiles were clearly separable. **B**: Volcano plot with the red and blue dots representing the up and down regulation of differentially expressed genes, respectively. **C**: GO bar chart showing significant accumulation: significantly enriched GO terms based on $P \leq 0.05$; the horizontal axis shows the Gene Ratio; the vertical axis shows the description of GO terms. **D**: GO term enrichment analysis and expression patterns of differentially expressed genes (DEGs).

neural and sensory functions. Notably enriched terms include "neuron-to-neuron synapse", "immune response-activating signaling pathway", "regulation of synapse structure or activity", and "sensory perception of sound". These findings suggest that the p.V37I mutation in aging mice affects synaptic and calcium signaling pathways, as well as sensory system development (Figure 3C, 3D).

4. Discussion

The *GJB2* gene mutation is the predominant cause of deafness and hearing loss, particularly in East Asia, where the p.V37I mutation is the most prevalent variant. A comprehensive cross-sectional study involving a full life-cycle population cohort with the biallelic p.V37I mutation demonstrated a steadily progressive hearing loss that increases in prevalence with age (*10*). This suggests that the p.V37I mutation may play a significant role in ARHL in humans. It is critical to develop appropriate animal models to explore the pathogenesis of hearing loss induced by gene mutations effectively. Interestingly, the expression and functional impact of the *GJB2* gene c.109G>A mutation differ between species. In human's gene, the c.109G>A substitution results p.V37I amino acid change. However, in mice, the analogous c.109G>A substitution results in a p.V37M amino acid change (Figure 1B, 1D), which leads to progressive, mild hearing loss without significant developmental or morphological abnormalities (*13,14*). This interspecies variability limits the translational relevance of current mouse models for studying the c.109G>A (p.V37I) mutation in humans. To address this limitation, we engineered a novel mouse model with a double-base edit in the p.V37 codon of the *GJB2* gene, successfully replicating the human p.V37I amino acid sequence. This modification accurately replicates the human p.V37I amino acid sequence, thereby enhancing the model's relevance for studying the mutation's effects. The c.109G>A mutation leads to a single amino acid change, in this study, it resulted in p.V37I in humans and p.V37M in mice. This genetically modified model allows for a closer examination of the mutation's pathophysiological effects and provides a valuable tool for investigating the mechanisms underlying ARHL and related hearing disorders. Compared to models carrying the p.V37M mutation, our p.V37I model also exhibited a progressive, mild-to-moderate hearing loss. Considering the different strain background and experimental equipment difference, the difference can be reasonable. Both variants are associated with a relatively mild form of hearing loss, indicating these mutations can cause nuanced impact on the auditory function.

In our study of cochlear development and the structure of the organ of Corti, we observed that p.V37I mice exhibited a phenotype indicative of very milder auditory impairment. Morphological analysis revealed no significant abnormalities in the cochlear structure or the organ of Corti (Figure 2B). SEM further confirmed the absence of significant microstructural changes in p.V37I mice compared to WT controls (Figure 2C). Compared to the findings reported from the p.V37M model (*13,14*), no significant differences in the length of gap junction plaques were observed between p.V37M and WT mice. On the other hand, more severe cochlear disruptions have been documented in studies of other *GJB2* mutations, such as c.235delC and Cx26 knockout (KO) mice, which include structural abnormalities like closure of the tunnel of Corti (*13,14,17,18*). These observations highlight the diverse impacts of different *GJB2* mutations on cochlear architecture and auditory function. Unlike mutations associated with congenital hearing loss, such as the R75W transgenic and certain conditional knockout models, the p.V37I mutation resulted in progressive rather than congenital hearing loss (*19*). This kind of hearing loss aligned with the absence of significant structural changes in the cochlea, suggesting a more subtle impact of the p.V37I mutation on cochlear integrity.

RNA-Seq is a widely used method in both laboratory research and clinical studies, as it provides a more accurate measurement of transcript levels and their isoforms than other methods, such as microarrays. To investigate the potential mechanisms behind the gene expression changes in the p.V37I mice, we conducted RNA-Seq analyses for both p.V37I and WT mice at different ages. ARHL is characterized as a degenerative condition in which crucial genes are progressively downregulated over time. In our study, p.V37I mice began to exhibit signs of hearing loss by 8 months of age, in contrast to their WT counterparts. PCA revealed that at a younger age, the gene expression profiles in the cochlea of p.V37I mutant mice closely resembled those of wild-type mice. However, as the mice aged, the gene expression profiles diverged significantly, enabling clear differentiation into two distinct groups (Figure 3A). By 8 months of age, the number of downregulated DEGs in p.V37I mice was markedly higher than at younger ages, suggesting an accelerated decline in key gene expression (Figure 3B). This trend suggested that changes in gene expression are closely associated with the observed phenotype of hearing loss. Notably, these changes in gene expression appear to be age-dependent, indicating a potential link between aging processes and the exacerbation of auditory impairments in p.V37I mice.

The GO enrichment analysis of the DEGs between aging p.V37I and aging WT mice revealed significant enrichment in biological processes related to neural and sensory functions. Notably enriched terms included "neuron-to-neuron synapse", "immune response-activating signaling pathway", "calcium-mediated signaling pathway", and "sensory perception of sound", (Figure 3C, 3D). These findings suggest that the p.V37I mutation in aging mice influences synaptic and calcium signaling pathways, as well as the sensory

system's development and function. Calcium (Ca^{2+}) signaling in the cochlea is well-established as critical for the development and maturation of outer hair cell afferent innervation (*20,21*). In p.V37I mutant cochleae, age-related changes in calcium signaling pathways may contribute to the functional decline of hair cells, ultimately leading to auditory impairment. On the other hand, the enrichment of the "immune response-activating signaling pathway" suggests that aging p.V37I cochleae may exhibit altered immune responses, potentially impacting their ability to resist external stimuli (*22*). These age-related changes in neural, calcium, and immune signaling pathways collectively provide insights into the mechanisms underlying the progressive hearing loss observed in p.V37I mice.

In conclusion, we conducted a comparative analysis of the transcriptional profiles of cochlea tissue between *GJB2* gene p.V37I mutant and the WT mice of different ages by RNA-Seq. We aimed to identify the underlying mechanisms of gene expression before any obviously morphological changes. The transcriptomic differences between the p.V37I and wild groups were different at different time points, indicating that the p.V37I mice may experience mild cochlea function impairment throughout their lifespan without experiencing observable hearing loss during their early years. However, as they age, the p.V37I mice become more vulnerable to oxidative stress, inflammation, immune system dysregulation, and other abnormalities compared to wild mice, leading to more severe age-related hearing loss. This is reflected by increased hearing impairment or earlier aging in old mice.

Moreover, it should be noted that the cochlea comprises a quite scarce number of sensory cells, and the bulk transcriptome sequencing approach is potentially insufficient for discerning the intricate gene expression patterns related to cilia and microtubules in outer hair cells (*23,24*). These specific gene expressions may be overshadowed by the influence of environmental noise. Consequently, further investigations are warranted to augment the depth of exploration into the inner ear, with particular emphasis on elucidating the functional characteristics and gene expression profiles of various cochlear systems, such as the Corti's organ and the stria vascular system (*25*). The employment of cutting-edge technologies and sequencing methodologies, such as single-cell sequencing, can help in deciphering the intricate mechanisms underlying genetic-induced hearing loss. Single-cell sequencing, boasting superior resolution capabilities when compared to bulk-seq, stands poised to represent the subsequent stride toward conducting more comprehensive and insightful research (*22,26,27*).

Acknowledgements

We sincerely appreciate the guidance of our tutors and every member of our team.

Funding: This work was supported by the National Natural Science Foundation of China (grant numbers 81870730, 82071064), and the Capital's Funds for Health Improvement and Research (grant number, CFH 2022-2-1092).

Conflict of Interest: The authors have no conflicts of interest to disclose.

References

1. World Health Organization. World report on hearing. *https://www.who.int/publications/i/item/world-report-on-hearing* (accessed January 19, 2025).
2. Cui Q, Chen N, Wen C, Xi J, Huang L. Research trends and hotspot analysis of age-related hearing loss from a bibliographic perspective. Front Psychol. 2022; 13:921117.
3. Salvi R, Ding D, Jiang H, Chen GD, Greco A, Manohar S, Sun W, Ralli M. Hidden age-related hearing loss and hearing disorders: Current knowledge and future directions. Hear Balance Commun. 2018; 16:74-82.
4. Lin FR, Yaffe K, Xia J, Xue QL, Harris TB, Purchase-Helzner E, Satterfield S, Ayonayon HN, Ferrucci L, Simonsick EM. Hearing loss and cognitive decline in older adults. JAMA Intern Med. 2013; 173:293-299.
5. Ahmadmehrabi S, Brant J, Epstein DJ, Ruckenstein MJ, Rader DJ. Genetics of postlingual sensorineural hearing loss. Laryngoscope. 2021; 131:401-409.
6. Wells HRR, Newman TA, Williams FMK. Genetics of age-related hearing loss. J Neurosci Res. 2020; 98:1698-1704.
7. del Castillo FJ, del Castillo I. The DFNB1 subtype of autosomal recessive non-syndromic hearing impairment. Front Biosci Landmark Ed. 2011; 16:3252-3274.
8. Li L, Lu J, Tao Z, Huang Q, Chai Y, Li X, Huang Z, Li Y, Xiang M, Yang J, Yao G, Wang Y, Yang T, Wu H. The p.V37I exclusive genotype of *GJB2*: A genetic risk-indicator of postnatal permanent childhood hearing impairment. PLoS One. 2012; 7:e36621.
9. Yu X, Lin Y, Xu J, Che T, Li L, Yang T, Wu H. Molecular epidemiology of Chinese Han deaf patients with bi-allelic and mono-allelic *GJB2* mutations. Orphanet J Rare Dis. 2020; 15(1):29.
10. Chen Y, Wang Z, Jiang Y, *et al*. Biallelic p.V37I variant in GJB2 is associated with increasing incidence of hearing loss with age. Genet Med. 2022; 24:915-923.
11. Wen C, Yang X, Cheng X, *et al*. Optimized concurrent hearing and genetic screening in Beijing, China: A cross-sectional study. Biosci Trends. 2023; 17:148-159.
12. Dai P, Huang LH, Wang GJ, *et al*. Concurrent hearing and genetic screening of 180,469 neonates with follow-up in Beijing, China. Am J Hum Genet. 2019; 105:803-812.
13. Chen Y, Hu L, Wang X, Sun C, Lin X, Li L, Mei L, Huang Z, Yang T, Wu H. Characterization of a knock-in mouse model of the homozygous p.V37I variant in Gjb2. Sci Rep. 2016; 6:33279.
14. Lin X, Li G, Zhang Y, Zhao J, Lu J, Gao Y, Liu H, Li GL, Yang T, Song L, Wu H. Hearing consequences in Gjb2 knock-in mice: implications for human p.V37I mutation. Aging. 2019; 11:7416-7441.
15. Chomczynski P, Sacchi N. The single-step method of RNA isolation by acid guanidinium thiocyanate-phenol-

chloroform extraction: twenty-something years on. Nat Protoc. 2006; 1:581-585.
16. Love MI, Huber W, Anders S. Moderated estimation of fold change and dispersion for RNA-seq data with DESeq2. Genome Biol. 2014; 15:550.
17. Zhu Y, Zong L, Mei L, Zhao HB. Connexin26 gap junction mediates miRNA intercellular genetic communication in the cochlea and is required for inner ear development. Sci Rep. 2015; 5:15647.
18. Li Q, Cui C, Liao R, *et al*. The pathogenesis of common *Gjb2* mutations associated with human hereditary deafness in mice. Cell Mol Life Sci. 2023; 80:148.
19. Inoshita A, Iizuka T, Okamura H-O, Minekawa A, Kojima K, Furukawa M, Kusunoki T, Ikeda K. Postnatal development of the organ of Corti in dominant-negative *Gjb2* transgenic mice. Neuroscience. 2008; 156:1039-1047.
20. Yang Y, Murtha K, Climer LK, Ceriani F, Thompson P, Hornak AJ, Marcotti W, Simmons DD. Oncomodulin regulates spontaneous calcium signaling and maturation of afferent innervation in cochlear outer hair cells. J Physiol. 2023; 601:4291-4308.
21. Murtha KE, Yang Y, Ceriani F, Jeng JY, Climer LK, Jones F, Charles J, Devana SK, Hornak AJ, Marcotti W, Simmons DD. Oncomodulin (OCM) uniquely regulates calcium signaling in neonatal cochlear outer hair cells. Cell Calcium. 2022; 105:102613.
22. Sun G, Zheng Y, Fu X, *et al*. Single-cell transcriptomic atlas of mouse cochlear aging. Protein Cell. 2023; 14:180-201.
23. Ma X, Guo J, Tian M, Fu Y, Jiang P, Zhang Y, Chai R. Advance and application of single-cell transcriptomics in auditory research. Neurosci Bull. 2024; 40:963-980.
24. Jean P, Wong Jun Tai F, Singh-Estivalet A, *et al*. Single-cell transcriptomic profiling of the mouse cochlea: An atlas for targeted therapies. Proc Natl Acad Sci. 2023; 120:e2221744120.
25. Xu Z, Tu S, Pass C, Zhang Y, Liu H, Diers J, Fu Y, He DZZ, Zuo J. Profiling mouse cochlear cell maturation using 10× Genomics single-cell transcriptomics. Front Cell Neurosci. 2022; 16:962106.
26. Liu H, Giffen KP, Chen L, Henderson HJ, Cao TA, Kozeny GA, Beisel KW, Li Y, He DZ. Molecular and cytological profiling of biological aging of mouse cochlear inner and outer hair cells. Cell Rep. 2022; 39:110665.
27. Hoa M, Olszewski R, Li X, Taukulis I, Gu S, DeTorres A, Lopez IA, Linthicum FH Jr, Ishiyama A, Martin D, Morell RJ, Kelley MW. Characterizing adult cochlear supporting cell transcriptional diversity using single-cell RNA-seq: Validation in the adult mouse and translational implications for the adult human cochlea. Front Mol Neurosci. 2020; 13:13.

Received January 29, 2025; Revised April 21, 2025; Accepted April 23, 2025.

**Address correspondence to:*
Lihui Huang, Otolaryngology Head and Neck Surgery, Beijing Tongren Hospital, Capital Medical University, Beijing 100730, China; Beijing Institute of Otolaryngology, Beijing 100005, China; Key Laboratory of Otolaryngology Head and Neck Surgery, Ministry of Education, Beijing 100005, China.
E-mail: huangpub@126.com

Ning Yu, College of Otolaryngology Head and Neck Surgery, Chinese PLA General Hospital, Beijing 100853, China; National Clinical Research Center for Otolaryngologic Diseases, Beijing 100853, China.
E-mail: yuning@301hospital.org

Released online in J-STAGE as advance publication April 28, 2025.